Journal of Applied Mechanics and Technical Physics, Vol. 47, No. 1, pp. 1–11, 2006

NUMERICAL STUDY OF THE NEAR-WALL GAS–DROPLET JET IN A TUBE WITH A HEAT FLUX ON THE SURFACE

V. I. Terekhov and M. A. Pakhomov

UDC 536.24

A model for calculating the flow of a turbulent mixture of air and suspended liquid particles injected into the near-wall region is developed within a unified approach of mechanics of heterogeneous media in the two-velocity and two-temperature approximation of the Eulerian approach. The influence of droplet evaporation in the near-wall jet on heat transfer between the two-phase gas–droplet flow and the wall is studied in the case of heat addition to the latter.

Key words: *gas–droplet near-wall screen, two-fluid model, evaporation, nonadiabatic surface.*

Introduction. Because of a permanent growth of temperatures of working media in heat-loaded elements of power engineering installations, the search for new methods of thermal protection of working surfaces is an urgent problem in aeromechanics and thermophysics.

An efficient method of protecting the tube wall is injection of a two-phase coolant through tangential slots (near-wall screens). The basic mechanism of improving thermoprotective properties of two-phase gas–droplet systems is the use of energy of the phase change that occurs near the wall.

Though the process of turbulent transport in multi-species systems is rather complicated, a certain progress is achieved in the development of numerical methods for calculating two-phase gas–droplet screens [1–4]. Available integral approaches to the theoretical description of the problem, which were developed in [1, 2], however, are based on a large number of simplifying assumptions that require detailed justification. Models based on systems of differential boundary-layer equations for a two-phase two-species mixture [3–5] are free from most of the drawbacks of these approaches. Numerical models offer a more detailed allowance for the specific features of heat and mass transfer in near-wall gas–droplet jets. In such a formulation, the problem of heat and mass transfer in the near-wall gas–droplet screen on an adiabatic surface was solved in [3, 4]. The main attention in these papers was paid to studying the influence of various factors (content of the liquid phase, injection parameter, nonisothermality, and droplet diameter) on the change in temperature of the adiabatic wall, which directly determines the thermal efficiency of the screen:

$$\Theta = (T_0 - T_{\mathrm{w}}^*)/(T_0 - T_{\mathrm{s}}).$$

Here T_0, T_{s}, and T_{w}^* are the temperatures of the main flow, the gas injected through the slot, and the adiabatic wall, respectively. The results obtained are in good agreement with the experimental data of [6, 7] on the magnitude of Θ and distributions of parameters over the jet cross section. The numerical and experimental investigations [1–4, 6, 7] revealed a significant increase in cooling efficiency (by a factor of 1.5 to 2) for the gas–droplet near-wall screen, as compared with a single-phase screen, with comparatively small contents of the liquid phase in the injected jet [up to 10% (by weight)].

In most cases in practice, surfaces are cooled by a hybrid approach combining local injection of the coolant into the near-wall region and regenerative heat transfer through the wall. In calculating the boundary layer with

Kutateladze Institute of Thermophysics, Siberian Division, Russian Academy of Sciences, Novosibirsk 630090; terekhov@itp.nsc.ru; pakhomov@ngs.ru. Translated from Prikladnaya Mekhanika i Tekhnicheskaya Fizika, Vol. 47, No. 1, pp. 5–17, January–February, 2006. Original article submitted February 1, 2005; revision submitted May 11, 2005.

0021-8944/06/4701-0001

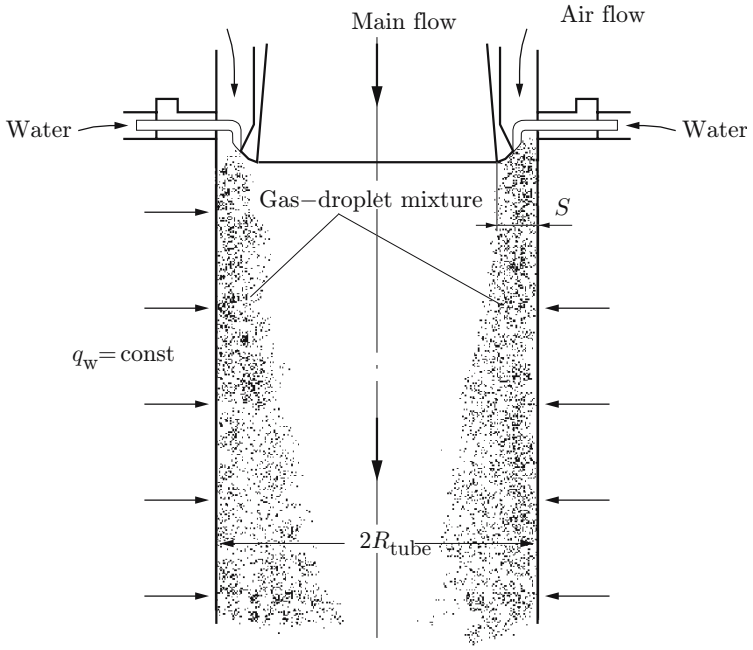

Fig. 1. Propagation of the near-wall gas–droplet jet in a tube with heated walls.

hybrid cooling, the heat-transfer coefficient in the gas-screen region is determined by the formula [8, 9]

$$\alpha^* = q_w/(T_w^* - T_w), \tag{1}$$

where q_w is the heat-flux density and T_w is the temperature of the wall without heat transfer through the wall. The use of T_w^* in Eq. (1) allows taking into account the influence of the near-wall jet on heat transfer. Such an approach significantly simplifies solving the problem of hybrid cooling and is widely used for heat-transfer analysis in various difficult situations [10–14]. The possibility of using this method for heat-transfer analysis in two-phase gas–droplet flows is an important issue in the heat-transfer theory, but there are no available data on the effect of two-phase near-wall screens in the case of heat exchange with the tube surface.

In the present paper, we consider the flow and heat transfer in the case of injection of a near-wall two-phase jet into a cocurrent gas flow with heat exchange on the tube surface with allowance for interphase interaction, stochastic motion of the mixture, and turbophoresis. The near-wall jet and the main flow are directed downward. The models of motion of the gas and disperse phases are constructed within the Eulerian approach [15–18] and basically agree with the numerical model of [5]. A substantial advantage of two-fluid models [3–5, 15–18], as compared with the Lagrangian approach, is the use of equations of the same type for both phases and, hence, a single algorithm for solving these equations. The description of the dynamics of a fine admixture causes no difficulties either, because a decrease in the size of disperse-phase particles leads to the limiting transition to the problem of turbulent diffusion of an inertia-free admixture.

Cases with a low injection parameter $m < 1$ with laws of near-wall turbulence prevailing in the evolution of the near-wall jet [14], and with a high injection parameter ($m > 1$) with prevailing jet-type mixing [13] are considered in the paper. The injection parameter m is determined as the ratio $\rho_s U_s/\rho_0 U_0$, where ρ is the density and U is the axial velocity of the flow; the subscripts "s" and 0 refer to parameters in the near-wall jet injected through the slot and in the main flow.

Formulation of the Problem. The evolution of the near-wall jet is shown in Fig. 1. The global flow consists of two coaxial flows. The hot main flow with a temperature T_0 is injected through the central tube of diameter $2(R_{tube} - S)$. The velocity distribution is assumed to be uniform, and air can be either dry or wet with a constant humidity φ_1 over the cross section. A peripheral annular slot of height S is used to inject the gas–vapor–droplet flow with a uniform distribution of all parameters both over the slot height and over its circumference. The vapor–liquid mixture at the slot exit can be either in the equilibrium state with both vapor and droplets being at the saturation line or in the nonequilibrium state with different phase temperatures.

The volume concentration of the liquid phase is low ($\Phi < 10^{-4}$), and the droplets are of moderate size (the initial diameter is $d_1 < 100$ μm). The processes in the flow do not include droplet coalescence (because of the small amount of the disperse phase) and droplet fragmentation (the Weber number $\mathrm{We} = \rho|\boldsymbol{U} - \boldsymbol{U}_{\mathrm{liq}}|d_1/\sigma \ll 1$ based on the droplet size and interphase velocity is much smaller than unity, whereas the critical Weber number is $\mathrm{We}_* = 7$, which follows from the data of [19]). Here σ is the surface tension; the subscript "liq" indicates the liquid phase. As was noted in [17], the effect of particle collisions in a two-phase flow can be neglected for the range of concentrations used. It is assumed that the droplets deposited onto the wall from the two-phase flow evaporate instantaneously, and the surface of the tube wall always remains dry, which is fairly valid for tubes with heated walls. This is supported by experimental [19] and numerical [5, 20] data. The particle concentration permanently decreases in the downstream direction because of deposition of particles onto the wall and jet expansion. The droplet size is a variable quantity both along the tube and over its cross section because of the difference in evaporation intensity depending on the local temperature of the gas phase. The droplet temperature over its radius is assumed to be constant.

System of Equations for the Gas Phase. Based on the assumptions used, the system of equations for an axisymmetric case of a two-phase gas–droplet flow in the boundary-layer approximation has the following form:

$$U\frac{\partial U}{\partial x} + \frac{1}{r}\frac{\partial (rV)}{\partial r} = \frac{6J\Phi}{\rho d},$$

$$\rho\Big[U\frac{\partial U}{\partial x} + \frac{V}{r}\frac{\partial (rU)}{\partial r}\Big] = -\frac{\partial P}{\partial x} + \frac{\rho}{r}\frac{\partial}{\partial r}\Big[r(\mu+\mu_{\mathrm{t}})\frac{\partial U}{\partial r}\Big] - \frac{3\Phi(U-U_{\mathrm{liq}})}{4d}C_{\mathrm{d}}\rho|\boldsymbol{U}-\boldsymbol{U}_{\mathrm{liq}}|,$$

$$\rho C_p\Big[U\frac{\partial T}{\partial x} + \frac{V}{r}\frac{\partial (rT)}{\partial r}\Big] = \frac{1}{r}\frac{\partial}{\partial r}\Big[r\Big(\frac{\mu}{\mathrm{Pr}} + \frac{\mu_{\mathrm{t}}}{\mathrm{Pr}_{\mathrm{t}}}\Big)\frac{\partial T}{\partial r}\Big] - \frac{\alpha}{d}(T - T_{\mathrm{liq}}) + \rho D\frac{\partial K_{\mathrm{vap}}}{\partial r}(C_{p,\mathrm{vap}} - C_{p,\mathrm{air}})\frac{\partial T}{\partial r}, \qquad (2)$$

$$\rho\Big[U\frac{\partial K_{\mathrm{vap}}}{\partial x} + \frac{V}{r}\frac{\partial (rK_{\mathrm{vap}})}{\partial r}\Big] = \frac{1}{r}\frac{\partial}{\partial r}\Big[r\Big(\frac{\mu}{\mathrm{Sc}} + \frac{\mu_{\mathrm{t}}}{\mathrm{Sc}_{\mathrm{t}}}\Big)\frac{\partial K_{\mathrm{vap}}}{\partial r}\Big] + \frac{J\Phi}{d},$$

$$\rho = \frac{P}{RT}, \qquad \frac{\partial P}{\partial r} = 0.$$

Here λ, μ, and D are the thermal conductivity, dynamic viscosity, and molecular diffusion of vapor to the gas, x and r are the axial and radial coordinates, respectively, V is the radial component of velocity of the vapor–gas mixture, C_p is the specific heat, C_{d} is the drag coefficient of the droplets, α is the heat-transfer coefficient of the evaporating droplet [20], T is the temperature, K_{vap} is the vapor concentration in the binary vapor–gas mixture, P is the pressure, J is the transverse mass flux of vapor from the surface of the evaporating droplet, R is the gas constant of the vapor–gas mixture, and Pr and Sc are the Prandtl and Schmidt numbers. The subscripts "air" and "vap" refer to air and vapor, respectively; turbulent characteristics are marked by the subscript "t."

The equations of continuity, energy, and diffusion contain the source and sink terms modeling the effect of the droplets on the transport processes, and the equation of motion has an additional term responsible for dynamic interaction between the phases.

The values of the turbulent Prandtl and Schmidt numbers were assumed to be constant over the tube length and radius and to be identical: $\mathrm{Pr}_{\mathrm{t}} = \mathrm{Sc}_{\mathrm{t}} = 0.9$. The Lewis number was assumed to be $\mathrm{Le} = \mathrm{Pr}/\mathrm{Sc} = 1$.

Two-Equation Model of Turbulence. Being modified to take into account the presence of the disperse phase, the equations of the turbulent kinetic energy k and its dissipation rate $\tilde{\varepsilon}$ have the form

$$\rho\Big[U\frac{\partial k}{\partial x} + \frac{V}{r}\frac{\partial (rk)}{\partial r}\Big] = \frac{\rho}{r}\frac{\partial}{\partial r}\Big[r\Big(\mu + \frac{\mu_{\mathrm{t}}}{\sigma_k}\Big)\frac{\partial k}{\partial r}\Big] + \Pi - \rho\varepsilon + \Pi_k + S_k,$$

$$\rho\Big[U\frac{\partial \tilde{\varepsilon}}{\partial x} + \frac{V}{r}\frac{\partial (r\tilde{\varepsilon})}{\partial r}\Big] = \frac{\rho}{r}\frac{\partial}{\partial r}\Big[r\Big(\mu + \frac{\mu_{\mathrm{t}}}{\sigma_\varepsilon}\Big)\frac{\partial \tilde{\varepsilon}}{\partial r}\Big] \qquad (3)$$

$$+ \frac{\tilde{\varepsilon}}{k}(C_{\varepsilon 1}f_1\Pi - C_{\varepsilon 2}\tilde{\varepsilon}\rho f_2) + \frac{0.79}{4}\frac{k^2}{\tilde{\varepsilon}}\frac{\partial U}{\partial x}\Big(\frac{V}{r}\Big)^2 + \Pi_\varepsilon + S_\varepsilon.$$

Here $\mu_{\mathrm{t}} = C_\mu f_\mu \rho k^2/\tilde{\varepsilon}$ and $\Pi = \mu_{\mathrm{t}}(\partial U/\partial r)^2$. The constants and damping functions were taken from [21].

The third term in the right side of the equation for turbulent energy dissipation takes into account extension of turbulent vortices for the case of an internal flow.

The terms S_k and S_ε, which characterize additional dissipation of gas-phase turbulence owing to the presence of small droplets, exchange of energy with the mean motion caused by averaged interphase slipping due to a nonuniform distribution of the droplet concentration, and influence of evaporation on gas turbulence are described in detail in [5].

System of Transport Equations for the Disperse Phase. One method of constructing the system of equations for disperse-phase motion and heat transfer is the use of the kinetic equation for the probability density function (PDF) for velocity and temperature of particles in a turbulent flow. The PDF equation is obtained under the assumption that fluctuations of velocity and temperature of the disperse phase are initiated by interaction of particles with turbulent fluctuations of the gas, which are modeled by Gaussian functions. Simulation of a real turbulent flow by a Gaussian process is rather approximate but yield good results from the viewpoint of practical applications. The kinetic equation for the PDF can be used to obtain a system of equations for modeling the dynamics and heat transfer of the disperse phase in the Eulerian continuum approach.

Equations of Momentum and Energy for Particles. Numerous recent studies show that the main forces acting on the droplet in a turbulent flow under conditions considered in the present problem are the aerodynamic drag, the force of gravity, and turbophoresis.

The system consisting of the continuity equation, equation for averaged components of velocity of the disperse flow in the axial (U_{liq}) and radial (V_{liq}) directions, and equation of energy in a cylindrical coordinate system is presented in the following form:

$$\frac{\partial\left(\Phi U_{\text{liq}}\right)}{\partial x}+\frac{1}{r}\frac{\partial\left(r\Phi V_{\text{liq}}\right)}{\partial r}=-\frac{6J\Phi}{\rho_{\text{liq}}d},$$

$$U_{\text{liq}}\frac{\partial U_{\text{liq}}}{\partial x}+\frac{V_{\text{liq}}}{r}\frac{\partial\left(rU_{\text{liq}}\right)}{\partial r}+\frac{\partial\left\langle v_{\text{liq}}^2\right\rangle}{\partial x}+\frac{1}{r\Phi}\frac{\partial}{\partial r}\left[r\Phi\langle u_{\text{liq}}v_{\text{liq}}\rangle\right]=\frac{U-U_{\text{liq}}\pm\tau g}{\tau}-\frac{D_{x,\text{liq}}}{\tau}\frac{\partial\ln\Phi}{\partial r},$$

$$U_{\text{liq}}\frac{\partial V_{\text{liq}}}{\partial x}+\frac{V_{\text{liq}}}{r}\frac{\partial\left(rV_{\text{liq}}\right)}{\partial r}+\frac{\partial\left\langle v_{\text{liq}}^2\right\rangle}{\partial r}=\frac{V-V_{\text{liq}}}{\tau}-\frac{D_{r,\text{liq}}}{\tau}\frac{\partial\ln\Phi}{\partial r}, \tag{4}$$

$$U_{\text{liq}}\frac{\partial T_{\text{liq}}}{\partial x}+\frac{V_{\text{liq}}}{r}\frac{\partial\left(rT_{\text{liq}}\right)}{\partial r}+\frac{1}{r\Phi}\frac{\partial}{\partial r}\left(r\Phi\langle\theta v_{\text{liq}}\rangle\right)=\frac{6}{C_{p,\text{liq}}\rho_{\text{liq}}d}\left\{\alpha(T-T_{\text{liq}})-J[L+C_{p,\text{vap}}(T-T_{\text{liq}})]\right\}.$$

Here $\langle u_{\text{liq}}^2\rangle$ and $\langle v_{\text{liq}}^2\rangle$ are the root-mean-square fluctuations of the droplet velocity in the streamwise and crossflow directions, $\langle u_{\text{liq}}v_{\text{liq}}\rangle$ are the turbulent stresses in the disperse phase, $D_{x,\text{liq}}$ and $D_{r,\text{liq}}$ are the coefficients of turbulent diffusion of droplets in the axial and radial directions, caused by the random motion of particles and their entrainment by high-energy vortices of the gas flow [18], and $\langle\theta v_{\text{liq}}\rangle$ is the correlation between the fluctuations of the droplet temperature and velocity. The equations of disperse-phase velocity fluctuations in the streamwise and crossflow directions have the form given in [18].

Heat Transfer between the Tube Wall and the Droplets Deposited onto the Wall Surface. When the particles deposit onto the wall, some part of the heat flux is spent on their evaporation. We assume the possibility of superposition of heat fluxes, as in [5, 19, 20]. The equation of density of the heat flux supplied to the tube wall q_{w} is the sum of the densities of heat fluxes from the wall to the liquid droplets $q_{\text{w,liq}}$ and from the wall to the gas–vapor–droplet mixture $q_{\text{w,fluid}}$. The density of the heat flux from the wall to the droplets deposited on this wall is [19]

$$q_{\text{w,liq}}=\exp\left[1-(T_{\text{w}}/T_{\text{liq}})^2\right]V_{\text{liq,w}}\rho_{\text{liq}}LM_{\text{liq},m},$$

where $M_{\text{liq},m}$ is the mean-mass concentration of droplets.

System (2)–(4) was supplemented by the equations of conservation of the sum of components of the gas–vapor–droplet mixture along the tube.

Boundary Conditions. The conditions of symmetry were imposed at the tube centerline:

$$\frac{\partial T}{\partial r}=\frac{\partial K_{\text{vap}}}{\partial r}=\frac{\partial U}{\partial r}=V=\frac{\partial U_{\text{liq}}}{\partial r}=V_{\text{liq}}=\frac{\partial\left\langle u_{\text{liq}}^2\right\rangle}{\partial r}=\frac{\partial\left\langle v_{\text{liq}}^2\right\rangle}{\partial r}=\frac{\partial T_{\text{liq}}}{\partial r}=\frac{\partial k}{\partial r}=\frac{\partial\tilde{\varepsilon}}{\partial r}=0. \tag{5}$$

The conditions on the wall were the no-slip and impermeability conditions for the gas-phase velocity and the zero kinetic energy of the gas and its dissipation rate:

$$U = V = 0, \qquad \frac{\partial K_{\text{vap}}}{\partial r} = 0, \qquad k = \tilde{\varepsilon} = 0. \tag{6}$$

The boundary conditions for the squared fluctuations of the axial and radial velocities and disperse-phase temperature are [18]

$$\langle v_{\text{liq}}^2 \rangle \frac{\partial U_{\text{liq}}}{\partial r} = -\frac{2}{\tau} q_{\text{liq}} \nu_{\text{t}} \Big(\frac{\partial U}{\partial r}\Big)_{\text{w}}, \qquad V_{\text{liq,w}} = \Big(\frac{2}{\pi} \langle v_{\text{liq}}^2 \rangle\Big)^{1/2}, \qquad \frac{\partial \langle u_{\text{liq}}^2 \rangle}{\partial r} = 0,$$

$$\frac{\partial \langle v_{\text{liq}}^2 \rangle}{\partial r} = -\frac{V_{\text{liq,w}}}{\tau}, \qquad \Big(\frac{1}{\tau} - \frac{1}{\tau_\Theta}\Big)^{-1} \langle v_{\text{liq}}^2 \rangle \frac{\partial T_{\text{liq}}}{\partial r} = f_{\theta v} \langle tv \rangle_{\text{w}}, \tag{7}$$

where $\tau = \rho_{\text{liq}} d^2/(18\mu W)$ is the time of dynamic relaxation of particles with allowance for the deviation from Stokes' flow regime, $W = (1 + \text{Re}_{\text{liq}}^{2/3}/6)$, $\tau_\Theta = C_{p,\text{liq}} \rho_{\text{liq}} d^2/(12\lambda Y)$ is the time of thermal relaxation of droplets, $Y = (1 + 0.3\text{Re}_{\text{liq}}^{1/2}\text{Pr}^{1/3})$, $\text{Re}_{\text{liq}} = d\sqrt{(U - U_{\text{liq}})^2 + (V - V_{\text{liq}})^2}\,/\nu$ is the Reynolds number of the disperse phase based on the slip velocity of the phases, q_{liq} and $f_{\theta v}$ are the functions that describe involvement of particles into high-energy fluctuations of gas-phase velocity and temperature [18], and $\langle tv \rangle = -(\nu_{\text{t}}/\text{Pr}_{\text{t}})\,\partial T/\partial r$ is the turbulent heat flux in the carrier phase.

All parameters are uniformly distributed in the entrance cross section of the tube. The single-phase main flow $0 \leqslant r \leqslant (R_{\text{tube}} - S)$ is described by the equations

$$U = U_0; \qquad V = V_0; \qquad T = T_0; \qquad K_{\text{vap}} = K_{\text{vap1}}; \qquad k_0 = k_{01}; \qquad \tilde{\varepsilon} = \tilde{\varepsilon}_{01}. \tag{8}$$

For the two-phase gas–droplet jet $(R_{\text{tube}} - S) \leqslant r \leqslant R_{\text{tube}}$, we have

$$U = U_{\text{s,liq}} = U_{\text{s}}; \qquad V = V_{\text{s,liq}} = V_{\text{s}}; \qquad T = T_{\text{s,liq}} = T_1; \qquad M_{\text{liq}} = M_{\text{liq1}};$$

$$d = d_1; \qquad K_{\text{vap}} = K_{\text{vap1}}; \qquad k = k_{\text{s1}}; \qquad \tilde{\varepsilon} = \tilde{\varepsilon}_{\text{s1}}. \tag{9}$$

The droplets at the entrance have an identical size and an identical temperature. The gas-phase turbulence is assumed to be $\text{Tu}_{01} = 4\%$ in the main flow at the tube entrance and $\text{Tu}_{\text{s1}} = 7\%$ in the near-wall flow.

Numerical Implementation. *Parabolic equations.* The parabolic equations are solved by the method developed for boundary-layer flows in [22]. The difference scheme has the second-order accuracy in both directions. The system of difference equations is supplemented by the boundary conditions (5)–(9) and is solved by the marching method.

The equations of continuity of the liquid, disperse phase, and radial velocity of the droplets are hyperbolic-type equations. In the present work, they are solved by Keller's box method [23], which also has the second-order accuracy in both directions.

As the grid step in the crossflow direction is nonuniform, it would be more convenient to transform the coordinate r to solve the system of equations on a uniform grid in the computational domain. The conversion of coordinates described in [23] is fairly suitable for such a two-dimensional boundary-layer problem.

All computations were performed on a grid containing 201 nodes in the axial and radial directions. Methodical computations were also performed on a nested grid (301 nodes along the tube and 301 nodes over the tube radius). A further increase in the number of computational nodes did not lead to any significant improvement of the results obtained.

As the equations in system (2)–(4) are nonlinear, they were solved by an iterative method. The condition of convergence was $|I_i - I_{i-1}| < 10^{-5}$ (i is the iteration number; the quantity I could be U, k, $\tilde{\varepsilon}$, T, K_{vap}, U_{liq}, V_{liq}, $\langle u_{\text{liq}}^2 \rangle$, $\langle v_{\text{liq}}^2 \rangle$, or T_{liq}). The computations were finalized when the criterion was satisfied for all variables.

Testing of Numerical Data for a Single-Phase Gas Screen. The calculated momentum thickness δ^{**} is plotted in Fig. 2, which also shows, for comparison, the experimental data of [24–26] and the results predicted by the formula [12]

$$\frac{\delta^{**}}{\delta_{\text{s}}^{**}} = \Big[1 + 0.016\Big(\frac{\Delta x}{\text{Re}_{\Delta x}^{0.2} \delta_{\text{s}}^{**}}\Big)^{1.25}\Big]^{0.8}, \tag{10}$$

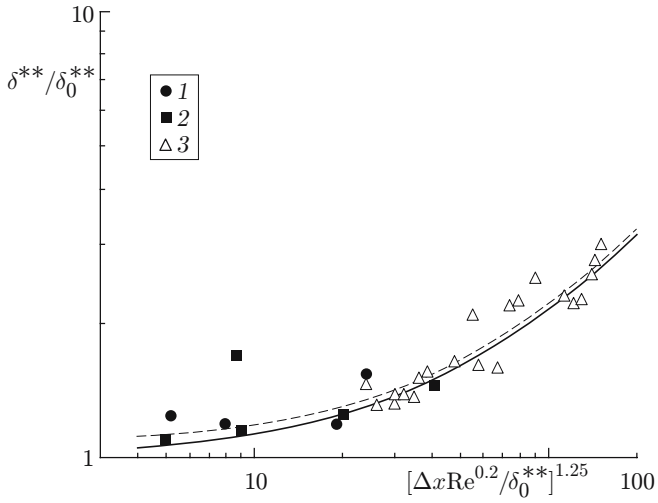

Fig. 2

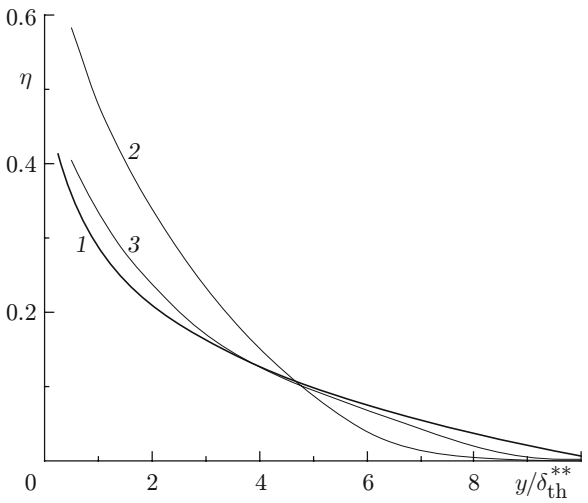

Fig. 3

Fig. 2. Momentum thickness in the case of injection of a single-phase jet: the solid and dashed curves show the results calculated by Eq. (10) and the present numerical model, respectively; the points are the experimental data of [24] (1), [25] (2), and [26] (3).

Fig. 3. Distribution of the gas temperature across the boundary layer: curve 1 refers to the calculation by formula $\eta = 1 - 0.715(y/\delta_{\mathrm{th}}^{**})^{1/7}$ and curves 2 and 3 refer to the calculations by formulas $\eta = (T_0 - T)/(T_0 - T_{\mathrm{w}})$ and $\eta = (T^* - T)/(T_{\mathrm{w}}^* - T_{\mathrm{w}})$, respectively.

where $\delta_{\mathrm{s}}^{**} = \int\limits_0^S \dfrac{\rho_{\mathrm{s}} U_{\mathrm{s}}}{\rho_0 U_0}\left(1 - \dfrac{U_{\mathrm{s}}}{U_0}\right) dy$ is the momentum thickness in the slot cross section and Δx is the streamwise coordinate counted from this cross section. It is seen in Fig. 2 that our data are in good agreement with the experimental results of [24–26] and with the calculations by Eq. (10).

The gas-temperature profiles in the presence of the heat flux on the surface are plotted in Fig. 3. Curve 1 is the exponential profile of the temperature defect with $n = 1/7$, which describes the temperature variation across a turbulent boundary layer under standard conditions [14]:

$$\eta = (T_0 - T)/(T_0 - T_{\mathrm{w}}) = 1 - 0.715(y/\delta_{\mathrm{th}}^{**})^{1/7}. \tag{11}$$

Curve 2 shows the numerical calculation where the difference between the main flow temperature T_0 and wall temperature in the presence of heat transfer T_{w} is used as the characteristic scale. Curve 3 depicts the calculation based on the difference between the adiabatic wall temperature T_{w}^* and the wall temperature in the presence of heat transfer T_{w}.

The energy thickness $\delta_{\mathrm{th}}^{**}$ was also determined by two methods: with the use of the difference between the wall temperature and the flow-core temperature in the presence of heat transfer $T_{\mathrm{w}} - T_0$ and the difference between the wall temperatures with and without heat transfer $T_{\mathrm{w}} - T_{\mathrm{w}}^*$.

As is seen in Fig. 3, the profile of the temperature defect calculated with the use of the adiabatic wall temperature (curve 3) almost coincides with the exponential distribution (11). The profile obtained on the basis of the temperature difference $T_{\mathrm{w}} - T_0$ (curve 2) lies significantly higher than dependence (11), which supports the validity of using the temperature difference $T_{\mathrm{w}} - T_{\mathrm{w}}^*$ in calculating heat transfer in the region of single-phase gas screens.

This fact is also evidenced by the calculations of heat transfer for the gas screen, which are plotted in Fig. 4 in the form of the Stanton number as a function of the integral Reynolds number. The values of St and $\mathrm{Re}_{\mathrm{th}}^{**}$ were determined on the basis of the temperature difference $T_{\mathrm{w}} - T_{\mathrm{w}}^*$:

$$\mathrm{St} = q_{\mathrm{w}}/(C_{p0}\rho_0 U_0 (T_{\mathrm{w}} - T_{\mathrm{w}}^*)), \tag{12}$$

$$\mathrm{Re}_{\mathrm{th}}^{**} = \rho_0 U_0 \delta_{\mathrm{th}}^{**}/\mu_0.$$

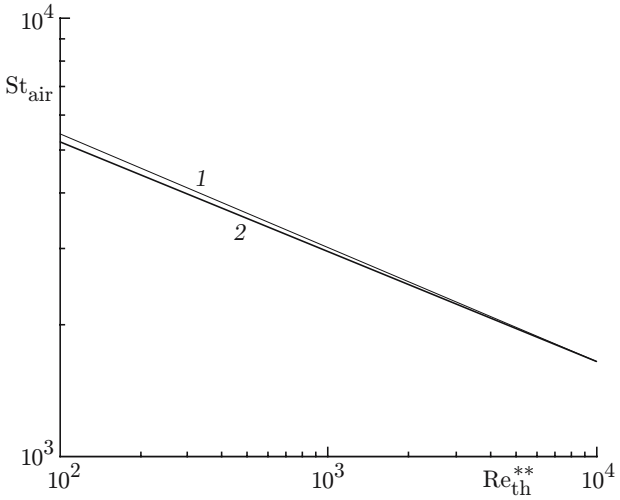

Fig. 4. Heat transfer in the gas screen: curves 1 and 2 show the calculations by the present numerical model and by Eq. (13), respectively.

It can be noted that the numerical results are in good agreement with the formula that describes heat transfer in a developed turbulent boundary layer [14]

$$\mathrm{St} = 0.0128(\mathrm{Re}_{\mathrm{th}}^{**})^{-1/4}\mathrm{Pr}^{-3/4}. \tag{13}$$

Calculation Results. All calculations were performed for a mixture of water and air in the following ranges of variation of the initial data: injection parameter $m = 0.1$–2, mass concentration of liquid droplets $M_{\mathrm{liq1}} = 0$–0.05, main flow temperature $T_0 = 323$–473 K, main flow velocity $U_0 = 50$ m/sec, and temperature of the two-phase flow at the slot exit $T_{\mathrm{s}} = T_1 = T_{\mathrm{liq1}} = 293$ K. The tube diameter was $2R_{\mathrm{tube}} = 0.1$ m, the slot height was $S = 5$ mm, the Reynolds number in the flow was $\mathrm{Re} = U_0 2R_{\mathrm{tube}}/\nu_0 = (1\text{–}3.5) \cdot 10^5$, the particle diameter varied within $d_1 = 0.1$–100 μm, and the Reynolds number of the droplet, which was based on the interphase velocity of the flow and on the initial size of the disperse phase, was $\mathrm{Re_{liq}} = d_1|\boldsymbol{U} - \boldsymbol{U}_{\mathrm{liq}}|/\nu = 0.01$–$4$, which corresponds to the limits of the Oseen flow. All calculations were performed under the condition of a constant heat flux on the wall $q_{\mathrm{w}} = \mathrm{const}$. The magnitude of the heat flux in different experiments varied within $q_{\mathrm{w}} = 5$–10 kW/m^2.

The effect of the mass concentration of droplets on heat transfer is illustrated in Fig. 5. The Stanton number was calculated by Eq. (12). The presence of evaporating droplets significantly (more than twofold) intensifies heat transfer in the gas–droplet near-wall flow owing to an increase in the number of droplets per unit volume. Even for the minimum value of the mass concentration (0.5% of the flow rate of the secondary air flow) can we see the presence of a two-phase zone at a small distance from the slot exit. The length of the enhanced heat-transfer region also depends on the liquid-phase concentration and significantly increases with increasing concentration.

It also follows from Fig. 5 that the use of the temperature difference $T_{\mathrm{w}} - T_{\mathrm{w}}^*$ as the characteristic scale does not allow generalization of data on heat transfer for the two-phase flow regime. This means that the equations of heat and mass transfer in the presence of phase changes become strongly nonlinear; hence, the approach developed in [8, 9] cannot be used for two-phase flows. All further calculations of the heat-transfer coefficients were performed with the use of the difference between the wall temperature and the flow-core temperature $T_{\mathrm{w}} - T_0$.

The influence of the main flow temperature T_0 on heat transfer between the tube wall and the gas–droplet screen is shown in Fig. 6 (here $\mathrm{St_{air}}$ is the Stanton number for a single-phase gas screen, other conditions being identical to those for the screen with heat transfer). As for two-phase near-wall screens on an adiabatic surface, the experiments [6, 7] and the calculations [3, 4] demonstrated a strong effect of the main flow temperature T_0 on heat- and mass-transfer processes. In the form shown in Fig. 6, the advantages of using a two-phase coolant over a single-phase gas flow can be directly identified. An increase in temperature of the main flow leads to a significant decrease in the value of $\mathrm{St} \,/\, \mathrm{St_{air}}$. This is explained by an increasing influence of evaporation processes with increasing T_0, which prevail at the outer edge of the mixing layer of the jet rather than in the vicinity of the wall.

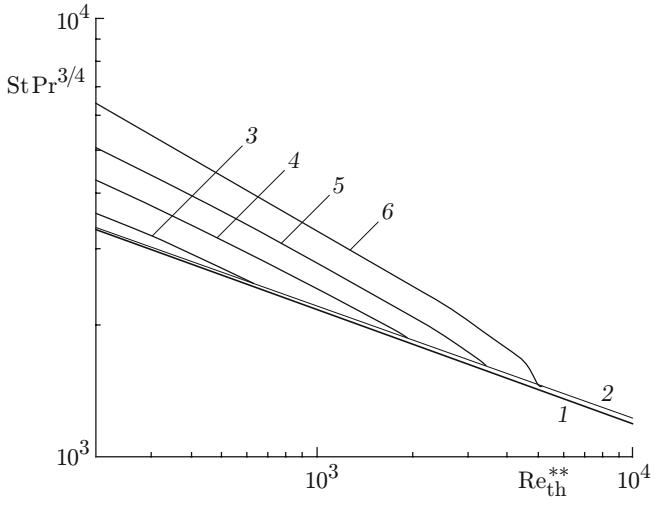

Fig. 5

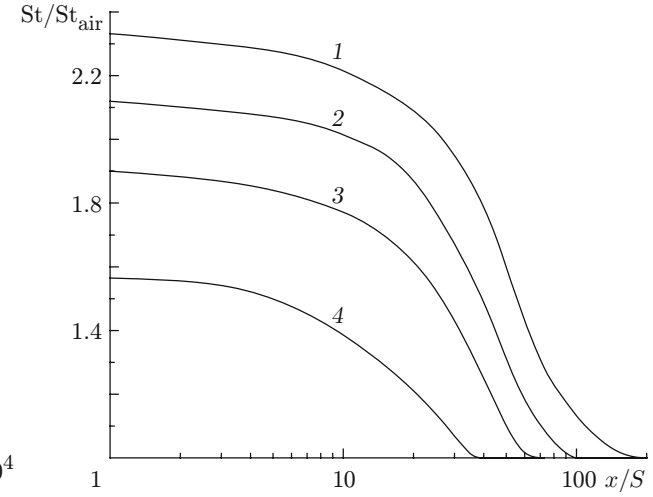

Fig. 6

Fig. 5. Effect of the droplet concentration on heat transfer in the two-phase near-wall jet ($q_{\mathrm{w}} = 5$ kW/m^2, $T_0 = 373$ K, $T_{\mathrm{s}} = T_1 = T_{\mathrm{liq1}} = 293$ K, $U_0 = 50$ m/sec, $d_1 = 30$ μm, $m = 0.8$, and $M_{\mathrm{vap1}} = 0.014$): curve 1 shows the calculation by Eq. (13); $M_{\mathrm{liq1}} = 0$ (2), 0.005 (3), 0.01 (4), 0.025 (5), and 0.05 (6).

Fig. 6. Variation of the heat-transfer coefficient along the tube for different temperatures of the main flow ($q_{\mathrm{w}} = 5$ kW/m^2, $T_{\mathrm{s}} = T_1 = T_{\mathrm{liq1}} = 293$ K, $U_0 = 50$ m/sec, $d_1 = 30$ μm, $m = 0.8$, $M_{\mathrm{vap1}} = 0.014$, and $M_{\mathrm{liq1}} = 0.05$): $T_0 = 323$ (1), 373 (2), 423 (3), and 473 K (4).

The effect of the injection parameter m on heat-transfer intensification is demonstrated in Fig. 7. Heat-transfer intensification ceases with increasing distance from the injection point, as the fraction of the droplet phase decreases in the downstream direction. Like the thermal efficiency Θ [12, 14], the quantity $\mathrm{St}\,/\,\mathrm{St_{air}}$ has a maximum. In contrast to Θ, however, whose maximum value is reached with the injection parameter $m = 1$, the maximum intensification in the two-phase flow is observed for $m = 1.5$–1.8.

Figure 8 shows the distributions of heat-transfer intensification in gas–droplet jets with a varied heat flux on the tube wall. As the heat flux increases, the value of $\mathrm{St}\,/\,\mathrm{St_{air}}$ decreases owing to more intense evaporation processes and faster removal of the liquid phase from the boundary layer near the wall, which reduces temperature gradients in the near-wall zone.

Data on variation of the particle size along the tube are very important for tube-surface cooling. Figure 9 shows the calculated mean-mass size of particles for different mass concentrations M_{liq1}, which was calculated as

$$d_m = \frac{2}{R^2_{\mathrm{tube}}} \int\limits_0^{R_{\mathrm{tube}}} d\,r\,dr.$$

As it follows from Fig. 9, the particle size monotonically decreases along the tube. The data in Fig. 9 allow us to determine the length of the evaporation zone, which increases with increasing droplet size.

The complicated laws of heat and mass transfer in near-wall gas–droplet jets can be analyzed by using local distributions of thermogasdynamic parameters across the boundary layer. Figure 10 shows the profiles of normalized concentrations (curve 1), droplet size (curve 2), gas temperature (curve 3), total enthalpy (curve 4), gas velocity (curve 5), and concentration of water vapor (curve 6).

The total enthalpy of the gas–droplet mixture was calculated by the formula

$$H = \sum_{i=1}^{3} H_i M_i = H_{\mathrm{air}} M_{\mathrm{air}} + H_{\mathrm{liq}} M_{\mathrm{liq}} + H_{\mathrm{vap}} M_{\mathrm{vap}},$$

where $H_i = \int C_{pi}\,dT_i + h_i^0$ is the enthalpy of the ith component with allowance for the energy of formation of the component from simple substances (h_i^0) and M_i is the mass concentration of the component.

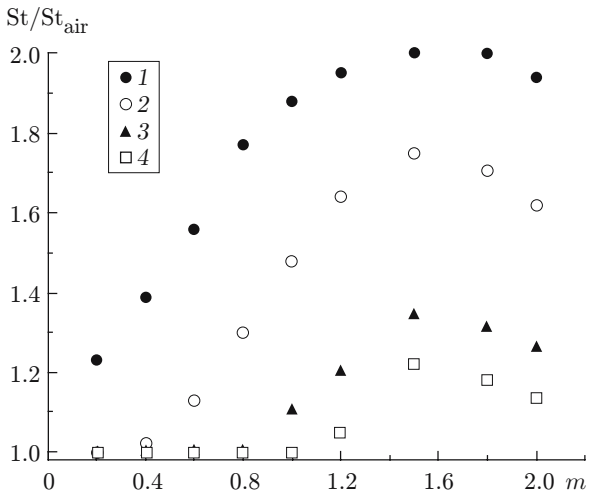

Fig. 7

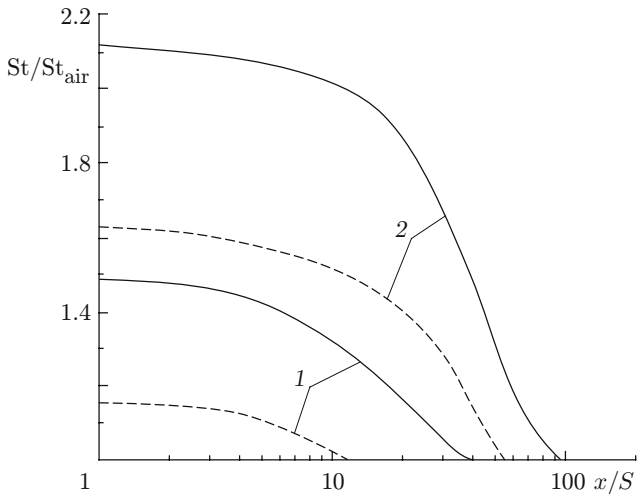

Fig. 8

Fig. 7. Effect of the injection parameter m on heat-transfer intensification: $x/S = 25$ (1), 50 (2), 100 (3), and 200 (4); the conditions the same as in Fig. 5.

Fig. 8. Heat transfer in the gas–droplet screen with a varied heat flux: $M_{\mathrm{liq1}} = 0.01$ (1) and 0.05 (2); the solid and dashed curves refer to $q_{\mathrm{w}} = 5$ and 10 kW/m^2, respectively; the conditions the same as in Fig. 5.

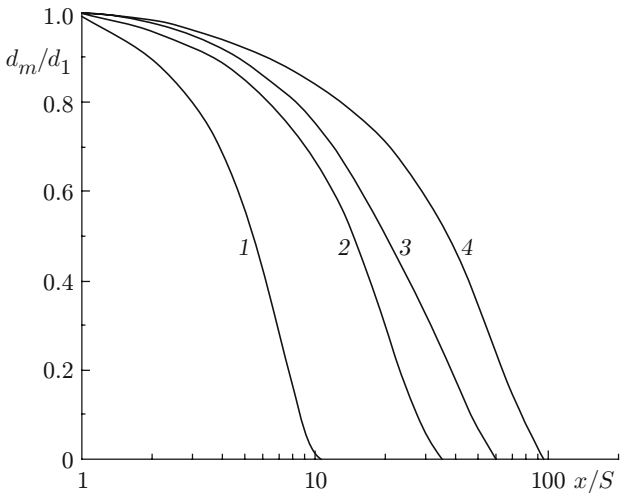

Fig. 9. Variation of the mean-mass size of the disperse phase along the tube: $M_{\mathrm{liq1}} = 0$ (1), 0.005 (2), 0.025 (3), 0.025 (4), and 0.05 (5); the conditions the same as in Fig. 5.

The points in Fig. 10 show the exponential ($n = 1/7$) distributions of parameters across the boundary layer. No similarity is observed in the distributions of parameters across the boundary layer. This could be expected, as the equations of motion, energy, and diffusion do not possess the property of similarity because of the presence of source terms caused by evaporation of liquid droplets. Note that a similar situation is also observed for near-wall gas–droplet screens above an adiabatic wall [3]. The profile of the mass concentration of vapor has a clearly expressed maximum: evaporation front located in the near-wall zone. If the heat flux is involved, the most intense evaporation processes occur in the vicinity of the wall. There is one more local maximum of the vapor concentration near the boundary of the screen–main flow mixing zone, which is caused by vapor release at the boundary of mixing with the hot external flow.

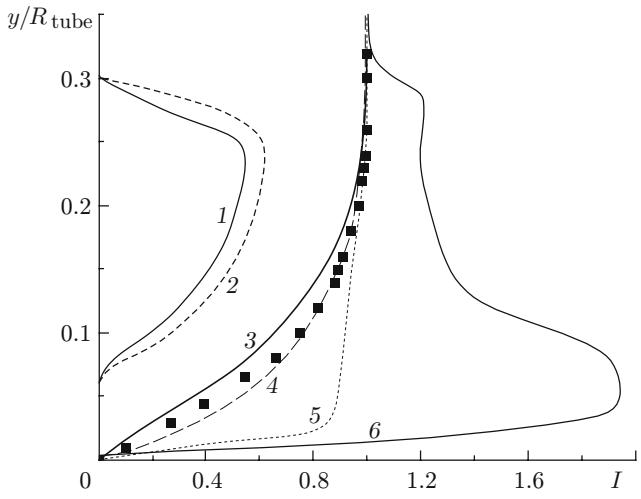

Fig. 10

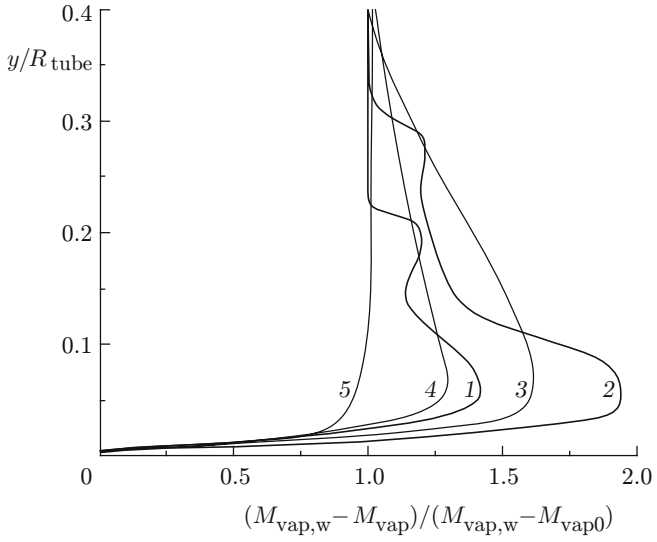

Fig. 11

Fig. 10. Distributions of parameters of the two-phase screen (I) over the tube cross section: $I = M_{\text{liq}}/M_{\text{liq1}}$ (1), $I = d/d_1$ (2), $I = \Theta$ (3), $I = \Theta_H$ (4), $I = U/U_0$ (5), and $I = (M_{\text{vap,w}} - M_{\text{w}})/(M_{\text{vap,w}} - M_0)$ (6); the points show the profile $\Theta = U/U_0 = (y/\delta_{\text{th}})^{1/7}$.

Fig. 11. Cross-sectional mass concentrations of vapor along the tube: $x/S = 25$ (1), 50 (2), 100 (3), 150 (4), and 200 (5).

Figure 11 shows the distributions of the mass concentration of vapor (which was uniform in the entrance cross section of the tube) in five cross sections along the tube. It is seen that the high gradients of the vapor concentration (curves 1 and 2) are leveled off in the downstream direction owing to the enhanced influence of diffusion processes and jet mixing.

Conclusions. A physical model of heat and mass transfer in the case of injection of a gas–droplet near-wall jet into a turbulent gas flow in a heated cylindrical tube is developed. The liquid phase in this model consists of localized sinks of heat and sources of vapor and interphase friction. The model takes into account droplet deposition onto the wall and heat transfer caused by the droplet–wall contact. The droplets deposited onto the wall are assumed to evaporate instantaneously so that no liquid film is formed on the wall surface. The turbulent characteristics of the gas phase were calculated with the use of the k–$\tilde{\varepsilon}$ model of turbulence.

The heat and mass transfer and the flow structure in propagation of the near-wall gas–droplet screen with heat addition is numerically examined in a wide range of variation of thermophysical parameters at the tube entrance.

Addition of droplets into the near-wall flow enhances the heat transfer (more than twofold) owing to the increased fraction of heat spent on the phase change and heat transfer due to the direct contact of droplets with the wall.

The rate of heat-transfer intensification is found to decrease with increasing temperature of the main flow and density of the heat flux on the wall.

It is demonstrated that the method for calculating heat transfer in single-phase gas screens, which is based on the adiabatic wall temperature as the governing parameter, is inapplicable for two-phase gas–droplet screens.

This work was supported by the Foundation "Leading Scientific Schools of Russia" (Grant No. NSh-1308.2003.8), Russian Foundation for Basic Research (Grant No. 05-02-16281a), and Russian Science Support Foundation (Grant for young candidates of sciences, 2005).

REFERENCES

1. A. A. Vasil'ev, "Efficiency of the gas–vapor–liquid heat screen behind a tangential slot," *Promyshl. Teplotekh.*, **10**, No. 4, 36–38 (1988).
2. V. M. Repukhov and A. I. Neduzhko, "Efficiency of the gas–vapor–liquid heat screen behind tangential slots," *Promyshl. Teplotekh.*, **11**, No. 4, 31–37 (1989).
3. V. I. Terekhov and M. A. Pakhomov, "The study of structure, heat and mass transfer in the gas–droplet near-wall jet in a tube," in: *Proc. 3rd Int. Symp. on Two-Phase Flow Modelling and Experimentation* (Pisa, Italy, May 30–June 4, 2004), Edizioni ETS, Pisa (2004); CD-ROM, Paper No. VEN 11.
4. V. I. Terekhov and M. A. Pakhomov, "The modeling of a tube flow with injection of near-wall non-isothermal turbulent gas–droplets jet," in: *Proc. 5th Int. Conf. on Multiphase Flow* (ISMF-2004), Yokohama, Japan, September 22–24 (2004); CD-ROM, Paper No. 135.
5. V. I. Terekhov and M. A. Pakhomov, "The numerical modeling of the tube turbulent gas-drop flow with phase changes," *Int. J. Therm. Sci.*, **43**, No. 6, 595–610 (2004).
6. V. I. Terekhov, K. A. Sharov, and N. E. Shishkin, "Experimental study of gas-flow mixing with a near-wall gas–droplet jet," *Teplofiz. Aéromekh.*, **6**, No. 3, 331–340 (1999).
7. V. I. Terekhov, K. A. Sharov, and N. E. Shishkin, "Thermoprotective properties of gas–droplet screens in a vertical cylindrical tube," *Izv. Ross. Akad. Nauk, Énergetika*, No. 6, 111–119 (2003).
8. B. A. Zhestkov, V. V. Glazkov, and M. D. Guseva, *Method for Calculating the Wall Temperature during Jet and Hybrid Cooling* [in Russian], Gostekhteoretizdat, Moscow (1955).
9. E. R. G. Eckert and R. M. Drake, *Analysis of Heat and Mass Transfer*, McGraw-Hill, New York (1959).
10. R. J. Goldstein, "Film cooling," in: *Advance in Heat Transfer-1971*, Academic Press, New York (1971), Vol. 7, pp. 321–378.
11. V. M. Repukhov, *Theory of Thermal Protection of the Wall by Gas Injection* [in Russian], Naukova Dumka, Kiev (1980).
12. É. P. Volchkov, *Near-Wall Gas Screens* [in Russian], Nauka, Novosibirsk (1983).
13. G. N. Abramovich, T. A. Girshovich, S. Yu. Krasheninnikov, et al., *Theory of Turbulent Jets* [in Russian], Nauka, Moscow (1984).
14. S. S. Kutateladze and A. I. Leont'ev, *Heat and Mass Transfer, and Friction in a Turbulent Boundary Layer* [in Russian], Énergoatomizdat, Moscow (1985).
15. D. A. Drew, "Mathematical modeling of two-phase flow," *Ann. Rev. Fluid Mech.*, **15**, 261–291 (1983).
16. A. A. Shraiber, L. B. Gavin, V. A. Naumov, et al., *Turbulent Gas-Suspension Flows* [in Russian], Naukova Dumka, Kiev (1987).
17. É. P. Volkov, L. I. Zaichik, and V. A. Pershukov, *Modeling the Combustion of Solid Fuels* [in Russian], Nauka, Moscow (1994).
18. I. V. Derevich, "Hydrodynamics and heat and mass transfer of particles in a turbulent flow of a gas suspension in a tube," *Teplofiz. Vys. Temp.*, **40**, No. 1, 86–99 (2002).
19. K. Mastanaiah and E. N. Ganic, "Heat transfer in two-component dispersed flow," *Trans. ASME, J. Heat Transfer*, **103**, No. 2, 300–306 (1981).
20. V. I. Terekhov and M. A. Pakhomov, "Numerical study of hydrodynamics and heat and mass transfer of a ducted gas–vapor–droplet flow," *J. Appl. Mech. Tech. Phys.*, **44**, No. 1, 90–101 (2003).
21. C. B. Hwang and C. A. Lin, "Improved low-Reynolds-number k–$\tilde{\varepsilon}$ model based on direct simulation data," *AIAA J.*, **36**, No. 1, 38–43 (1998).
22. I. Yu. Brailovskaya and L. A. Chudov, "Solving the boundary-layer equations by the difference technique," *Vych. Metody Programm.*, No. 1, 167–182 (1962).
23. C. A. J. Fletcher, *Computational Techniques for Fluid Dynamics*, Vol. 2, Springer-Verlag, Berlin (1988).
24. A. V. Lebedev and Yu. V. Shvaikovskii, "Experimental study of distributions of velocity and turbulent characteristics in the gas screen," *Teplofiz. Vys. Temp.*, **3**, No. 4, 569–576 (1965).
25. J. P. Hartnett, R. C. Birkebak, and E. R. G. Eckert, "Velocity distribution, temperature distributions, effectiveness, and heat transfer for air injected through a tangential slot into a turbulent boundary layer," *Trans. ASME, J. Heat Transf.*, **83**, 293–306 (1961).
26. R. A. Seban and L. H. Back, "Velocity and temperature profiles in turbulent boundary layers with tangential injection," *Trans. ASME, J. Heat Transfer*, **84** (1962).